Environmental Science & Technology

pubs.acs.org/est

Article

Phosphorus Interactions with Iron in Undisturbed and Disturbed Arctic Tundra Ecosystems

Matthew John Berens, Alexander Bryce Michaud, Erin VanderJeugdt, Imtiaz Miah, Frederick W. Sutor, David Emerson, William B. Bowden, Lauren Kinsman-Costello, Michael N. Weintraub, and Elizabeth M. Herndon*

Cite This: https://doi.org/10.1021/acs.est.3c09072

Read Online

ACCESS | Metrics & More | Article Recommendations | Supporting Information

ABSTRACT: Phosphorus (P) limitation often constrains biological processes in Arctic tundra ecosystems. Although adsorption to soil minerals may limit P bioavailability and export from soils into aquatic systems, the contribution of mineral phases to P retention in Arctic tundra is poorly understood. Our objective was to use X-ray absorption spectroscopy to characterize P speciation and associations with soil minerals along hillslope toposequences and in undisturbed and disturbed low-lying wet sedge tundra on the North Slope, AK. Biogenic mats comprised of short-range ordered iron (Fe) oxyhydroxides were prevalent in undisturbed wet sedge meadows. Upland soils and pond sediments impacted by gravel mining or thermokarst lacked biogenic Fe mats and were comparatively iron poor. Phosphorus was primarily contained in organic compounds in hillslope soils but associated with Fe(III) oxyhydroxides in undisturbed wet sedge meadows and calcium (Ca) in disturbed pond sediments. We infer that phosphate mobilized through organic decomposition binds to Fe(III) oxyhydroxides in wet sedge, but these associations are disrupted by physical disturbance that removes Fe mats. Increasing disturbances of the Arctic tundra may continue to alter the mineralogical composition of soils at terrestrial-aquatic interfaces and binding mechanisms that could inhibit or promote transport of bioavailable P from soils to aquatic ecosystems.

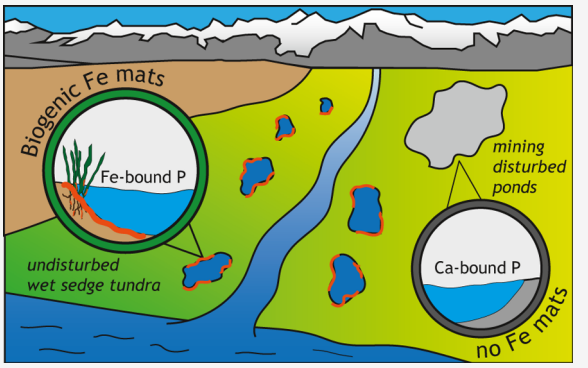

KEYWORDS: *phosphorus, soil disturbance, biogenic Fe mats, tundra soils, Fe redox cycling, X-ray absorption spectroscopy*

INTRODUCTION

Climate change is rapidly altering biogeochemical processes in northern high-latitude ecosystems. Permafrost thaw is releasing vast stores of previously frozen organic matter that can be decomposed and emitted as climate-warming greenhouse gases (i.e., CO_2 and CH_4).[1] Increases in plant productivity caused by warmer temperatures could partially offset these C losses,[1−3] but plant growth in Arctic ecosystems may be inhibited by low nutrient availability.[4] In particular, Arctic soils are often low in bioavailable phosphorus (P), namely inorganic orthophosphate anions, from occlusion of P in soil organic matter and the corresponding slow rates of P mineralization due to colder temperatures, i.e., enzymatic dephosphorylation of organic matter.[5−8] Yet, a full understanding of the factors influencing P bioavailability in Arctic tundra ecosystems is limited due to knowledge gaps in the occurrence, distribution, and speciation of reactive soil minerals that could bind and sequester phosphate.

Ferric iron (Fe) minerals adsorb large quantities of P (primarily as inorganic phosphate)[9−11] and may potentially limit its availability to plants and microorganisms. However, Fe(III) minerals are susceptible to reductive dissolution and solubilization during hydrologically driven redox cycles that can release P from soils into aquatic systems.[12,13] The susceptibility of Fe(III) minerals to dissolution is dependent on the physical size, composition, and crystallinity of the underlying mineral structure.[14] Phosphorus can also be immobilized by coprecipitation with calcium (Ca) carbonates and coprecipitation or sorption to aluminum (Al) oxides and clay minerals, potentially to a similar or greater extent than Fe oxides.[15−17] Conversely, the weathering and dissolution of Ca and Al phosphate minerals could release significant amounts of P previously bound to those minerals.[18−21] However, unlike Fe(III) (oxyhydr)oxides, the mechanism of dissolution of Ca carbonate, Al oxide, and clay minerals is not directly redox driven but more dependent on soil pH.[22,23] Thus, knowledge

Received: October 31, 2023
Revised: May 28, 2024
Accepted: May 29, 2024

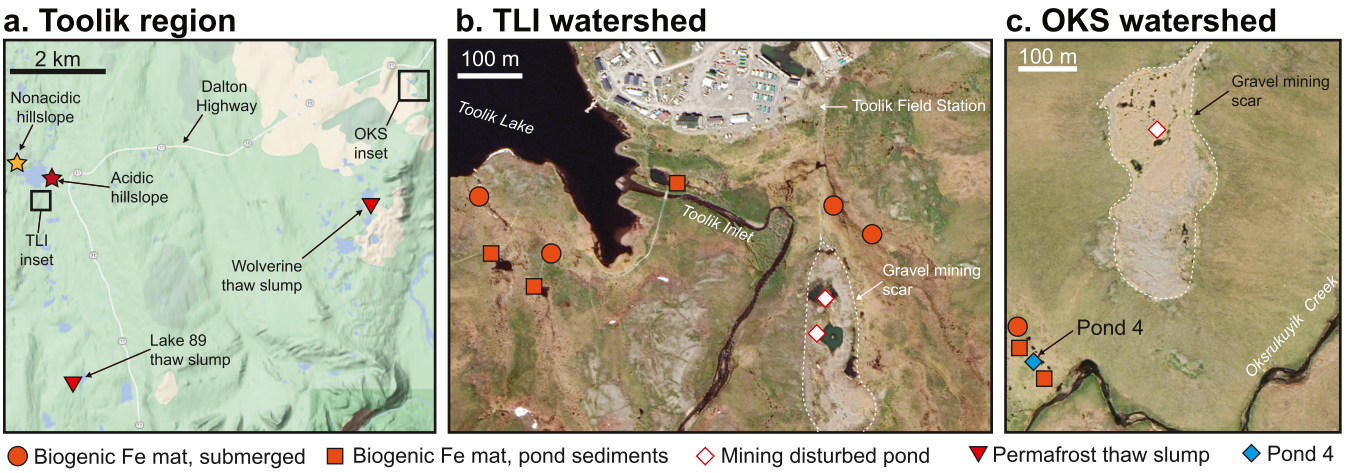

Figure 1. (a) Overview of all sampling locations with inset maps for (b) Toolik Lake Inlet (TLI) and (c) Oksrukuyik Creek (OKS) watersheds. (a) Hillslope transects and retrogressive permafrost thaw slumps are individually marked. (b, c) Mining-disturbed regions are indicated by the dotted line. A detailed list of all sampling locations is in Tables S1 and S2.

of the quantity and speciation of soil minerals that interact with P at terrestrial−aquatic interfaces is critical for evaluating the ability of soil at terrestrial−aquatic interfaces to be sources or sinks of bioavailable P, with implications for control of the ecosystem carbon balance in Arctic tundra.

Several studies have reported the widespread occurrence of Fe microbial mats on the surface of saturated, organic-rich tundra soils.[24−28] These biogenic Fe mats form through the activity of Fe(II)-oxidizing bacteria, which colonize soil environments where opposing iron and oxygen gradients supply dissolved Fe^{2+} and limit dissolved oxygen. Fe(II)-oxidizing bacteria form thin (~0.5−2 cm) coatings of short-range ordered Fe(III) oxyhydroxides (e.g., ferrihydrite) that comprise biogenic Fe mats.[26,29] Due to the high phosphate sorption capacity of biogenic Fe(III) oxyhydroxides,[9] biogenic Fe mats could form an unrecognized sink and barrier to P transfer across terrestrial-aquatic interfaces, which may contribute to P limitation either in soils or in adjacent aquatic systems. Although Fe cycling in Arctic systems has gained increasing attention,[27,30,31] there remains limited knowledge regarding the geochemical composition of biogenic Fe mats, their distribution on the landscape, and their ability to bind inorganic phosphate and potentially limit its bioavailability. To address this knowledge gap, we compared the geochemical compositions of organic-rich surface soils in upland, midslope, and lowland positions of two hillslope toposequences to biogenic Fe mats formed at terrestrial−aquatic interfaces of low-lying wet sedge tundra in the Alaska North Slope region. We also evaluated pond sediments in areas impacted by gravel mining and retrogressive thaw slumps to explore whether anthropogenic disturbance could influence the formation of biogenic Fe mats and consequently, the major pools of P present in Arctic surface environments.

METHODS

All work for this study was conducted in the field (sample collection) or laboratory (bulk geochemical and X-ray characterization) and no unexpected or significant safety hazards were encountered.

Site Description. The Toolik Field Station (68.66109, −149.37047, mean elevation 820 m) is located on the North Slope of Alaska. Maps of the Toolik region and individual study areas are shown in Figure 1. The region is underlain by continuous permafrost (~200 m depth) with a shallow active layer (~10−75 cm) that develops annually during the summer season.[32] Soils in this region are either acidic (pH < 6) and depleted in base cations (Ca, Mg, Na, K) or nonacidic (pH > 6), depending on the time since glaciation.[33] Land surfaces in the Toolik region are characterized by topographic-moisture gradients that span upland moist tussock tundra to relatively dry evergreen heath hilltops and lowland wet sedge meadows. The upland tussock tundra consists of thick organic soils with a maximum thaw depth of ~50 cm. The wet sedge lowlands are dominated by meadows of nontussock forming sedges (e.g., *Carex* spp., *Eriophorum* spp.) and series of interconnected ponds (<2 m depth) approximately 10−15 m apart that span from a few meters to tens of meters across.[24,34,35] The wet sedge meadows generally have thick organic horizons (~50 cm) that do not thaw to the mineral layer. The average gradient of vertical relief from tussock uplands to wet sedge lowlands is approximately 5−7 m over 50−250 horizontal meters.[32] To evaluate the variation in soil geochemical properties along typical hillslope toposequences in the Toolik region, we collected organic soils from upland, midslope, and lowland positions along an acidic and a nonacidic hillslope located on the east and west side of Toolik Lake, respectively (Figure 1a).

Biogenic Fe mats (n = 12) were collected from saturated wet sedge meadows within two small watersheds in the Toolik region (Figure 1a): the Toolik Lake Inlet (TLI) watershed and the Oksrukuyik Creek (OKS) watershed. Wet sedge meadows in the TLI watershed drain through a series of randomly distributed ponds directly into Toolik Lake. The OKS watershed (Figure 1c) is approximately 15 km ENE of the Toolik Field Station. Wet sedge meadows in the OKS watershed comprise a series of interconnected ponds that are likely precursors to a beaded stream that drains into Oksrukuyik Creek and ultimately into the Sagavanirktok River.[36] We collected "submerged" biogenic Fe mats from submerged plant materials in saturated soils and "pond" mats from sediment−water interfaces of small ponds within the wet sedge meadows. Pond sediments were collected from an additional four ponds in which biogenic Fe mats were absent, as confirmed by optical microscopy and DNA sequencing in

https://doi.org/10.1021/acs.est.3c09072
Environ. Sci. Technol. XXXX, XXX, XXX−XXX

Michaud et al.[24] Three of these ponds were formed on land surfaces excavated in the 1970s to extract mineral-rich gravel for construction of the Dalton Highway (notated as "mining-disturbed ponds" in Figure 1a). The fourth location (pond 4) was a pond with surface sediments dominated by a benthic diatom species. To our knowledge, there have been no disturbance events associated with pond 4. To evaluate natural disturbance events, surface sediments were collected from mud slurries forming adjacent to the thawing front of two retrogressive thaw slumps: Lake 89 and Wolverine (Figure 1a, Table S1).

Sample Collection. All biogenic Fe mats were collected in June and July 2019, except for one sample collected in August 2021 (Table S1). Five submerged and six pond biogenic Fe mats were collected in addition to surface sediments from three mining-disturbed ponds. Biogenic Fe mats were collected by aspirating the mat material with a sterile 25 mL serological pipet and transferring it into a sterile 15 mL conical centrifuge tube. Pond sediments in areas disturbed by gravel mining were collected by directly scooping out the top 1 cm of surface sediments with a sterile 50 mL conical tube. Retrogressive thaw slump samples were collected 5 m from the thaw slump headwall using a sterile 50 mL conical tube. All samples described above were preserved by freezing at −20 °C. The conical tubes containing the samples were vacuum-sealed in a plastic bag containing an oxygen-scrubbing packet (Anaero-Pack, Mitsubishi Chemical Corp.) to prevent oxidation during shipment to Bigelow Laboratory for Ocean Sciences. Hillslope soil cores (<20 cm depth) were collected in July 2021 from upland, slope, and lowland positions along hillslopes located in acidic (pH < 6) and nonacidic (pH > 6) tundra on either side of Toolik Lake. Intact cores were separated by the horizon (surface and subsurface organic) based on visual differences in texture and then frozen for shipment to the University of Tennessee. Sample information for all samples, including coordinates and collection dates, is in Tables S1 and S2.

Sample Preparation. The conical tubes containing biogenic Fe mat, disturbed pond sediment, and retrogressive thaw slump samples were transferred into a vinyl anaerobic chamber (5% H_2, 95% N_2, <1 ppm of O_2; Coy Laboratory Products) and allowed to thaw at room temperature. The thawed samples were centrifuged at 5000*g* for 15 min to concentrate the solid material, and the pellet was stored inside the anaerobic chamber in a desiccator containing freshly rejuvenated desiccant. The pellets were allowed to dry for 3 weeks (desiccant refreshed weekly) then sent to the Canadian Light Source for X-ray absorption spectroscopy (XAS) analysis (see below). Intact cores of surface and subsurface organic horizons were freeze-dried then homogenized by horizon prior to Fe XAS and bulk geochemical analysis. Phosphorus speciation was determined on subsamples of freeze-dried soils collected before homogenization; therefore, P speciation for hillslope soils represents P species present in the soil but may not be representative of the bulk soil composition.

Bulk Geochemical Analysis. The soil organic matter content was approximated from the loss-on-ignition (LOI, %) of oven-dried soils and sediments during combustion at 1000 °C for 4 h. Total element concentrations were determined by inductively coupled plasma atomic emission spectroscopy (ICP-AES) following lithium borate fusion of the combusted soils. LOI and ICP-AES analyses were conducted by ALS Geochemistry (Reno, NV). Although combustion at 1000 °C can include both soil organic matter and carbonates, carbonate contributions are expected to be low in these acidic, organic-dominated materials. Combined bulk geochemical results are provided in Table S3. The soil bulk density and gravimetric water content were determined for each soil horizon in hillslope soil cores. Soil bulk density was determined as the mass of dry soil after freeze-drying per soil volume calculated using the horizon depth and core diameter. Gravimetric water content was calculated as the mass of soil water, i.e., mass difference between the wet and freeze-dried soil, per mass of dry soil for each horizon. Soil bulk density ranged from 0.03 to 0.20 g soil·cm^{-3} (mean 0.08 g soil·cm^{-3}) and 0.06−0.23 g soil·cm^{-3} (mean 0.12 g soil·cm^{-3}) in the organic soils from the acidic and nonacidic hillslope, respectively. The gravimetric soil moisture content (mean ± SEM) was 4.4 ± 0.7 and 4.4 ± 0.6 g H_2O·g $soil^{-1}$ for acidic and nonacidic hillslopes, respectively.

Additional soil geochemistry from around the Toolik Field Station (TOOL) has been reported by the National Ecological Observatory Network (NEON).[37] We evaluated concentrations of oxalate-extractable Fe and Mehlich-III total P in all organic horizons (n = 31) collected during initial site characterization in August 2018 from 18 distributed plots spanning dwarf shrub and herbaceous sedge land covers. Oxalate-extractable Fe includes organically complexed and non- and semicrystalline Fe in addition to magnetite (Fe_3O_4) and minor amounts of crystalline Fe and trioctahedral Fe phyllosilicates and was used to represent SRO Fe(III)-oxyhydroxides measured in our study.[38−40] Mehlich-III total P is a measure of orthophosphate extractable by acetic acid and fluoride compounds and is used to represent total bioavailable P.[41]

X-ray Absorption Spectroscopy. Iron, P, and Ca K-edge X-ray absorption spectra were acquired for all biogenic Fe mat samples on beamline 06B1-1 Soft X-ray Microcharacterization Beamline (SXRMB) at the Canadian Light Source (CLS, Saskatoon, SK, Canada). Phosphorus spectra for the hillslope soils were also collected at SXRMB. Iron spectra for hillslope soils and Fe and P spectra for the thaw slump samples were performed at beamline 9-BM at the Advanced Photon Source (APS, Argonne National Laboratory, Argonne, IL). Samples for XAS analysis were dried and lightly ground with a mortar and pestle that were cleaned with methanol between each use. The powdered samples were transferred with a methanol-cleaned spatula onto C tape adhered to a Cu metal sample holder. Spectra were collected under vacuum in fluorescence and total electron yield (TEY) modes with a 7-element silicon drift detector. The distance from the sample to the detector was adjusted to optimize fluorescence counts for each element in each sample. Iron K-edge spectra were collected with energy steps of 5 eV from −88 to −8 eV, 0.35 eV from −8 to 40 eV, and 0.05 $Å^{-1}$ from 40 eV to 13 $Å^{-1}$ around the Fe K-edge. Fluorescence spectra were collected for environmental samples while total electron yield (TEY) spectra were collected for standards to avoid self-absorption effects. Phosphorus and Ca K-edge spectra were collected with energy steps of 2 eV from −20 to −6 eV, 0.15 eV from −6 to 20 eV, and 0.75 eV from 20 to 65 eV (P) or 100 eV (Ca). Phosphorus standards that were plotted in fluorescence were compared to TEY spectra, where available, to ensure consistent output between detectors. Spectra were deglitched, merged across replicate scans, and energy calibrated using *Athena* software.[42] The E_0 of each spectrum was set to the zero-crossing of the second derivative. All Fe spectra were shifted to align E_0 for the Fe reference foil

https://doi.org/10.1021/acs.est.3c09072
Environ. Sci. Technol. XXXX, XXX, XXX−XXX

collected during each run with that reported for a reference database (E_0 = 7110.75 eV).[43] No energy shift was applied to P spectra collected at CLS given that the P spectrum acquired for a $CaHPO_4$ standard was consistent with that reported in Hephaestus (v0.9.26).[42] Phosphorus spectra for thaw slump samples collected at APS were shifted by +3 eV to align with those collected at CLS. No energy shift was applied to Ca spectra since fitting was performed with standard spectra collected at the same beamline with the same energy calibration. Spectra were rebinned to 10 eV in the pre-edge region and 0.5 eV in the near edge X-ray absorption fine structure (NEXAFS) region to reduce noise, then baseline corrected using a linear regression in the pre-edge region and edge-step normalized using a second- or third-order polynomial to fit the postedge region. The normalization range for each P spectrum ranged from +27 ± 3 to +58 eV and was adjusted on the low end to ensure consistency and proper fitting, following Werner and Prietzel (2015). Files containing XANES and extended X-ray absorption fine structure (EXAFS) spectra and results of the linear combination fits are provided in the Supporting Information. The Fourier transformed Fe K-edge EXAFS spectra plotted in R space and the fitting results for P and Ca XANES spectra are shown in Figures S1−S5.

Average Fe oxidation states were determined using linear combination fits to $\mu(E)$ from −20 to +30 eV around the Fe K-edge with single-valence Fe standard compounds, i.e., biotite, vivianite, chlorite, Fe(II)-oxalate, Fe(III)-oxalate, Fe(III)-citrate, ferrihydrite, goethite, and hematite. Relative proportions of Fe(II) and Fe(III) were calculated as the sum of contributions from Fe(II) or Fe(III) standard compounds, respectively. Iron speciation was investigated using linear combination fits to $k^2\,\chi(\kappa)$ from 3 to 10 $Å^{-1}$. Each spectrum was fit with all combinations of select standards using up to five standards. The best fit for each spectrum was selected as the fit with the minimum number of components that were within 10% of the best fit, using reduced chi-square (χ^2) as a fitting parameter. If multiple fits met those criteria, the contributions of individual components were averaged across the best fits, and uncertainty was calculated as the standard error of the mean. In this approach, components were excluded if their addition did not significantly improve the fit. Best fit spectra were obtained with a single linear combination fit using the components reported by combinatorial fitting (Table S5). The final Fe components that contributed to the best fits were Fe(II)-bearing clays (chlorite (ripidolite)), crystalline Fe(III) oxides (goethite, magnetite), short-range ordered Fe(III) oxyhydroxides (lepidocrocite, 6L-ferrihydrite), and organic-bound Fe(III) (Fe(III)-citrate). Vivianite ($Fe(II)_3(PO_4)_2 \cdot 8H_2O$) and Fe(III) phosphate were included as components in linear combination fits for samples with P/Fe molar ratios >5% of total Fe (n = 16 total samples).

Phosphorus speciation was investigated using linear combination fits to $\mu(E)$ from −20 to +30 eV around the P K-edge. Standards used in the fits included organic phosphorus (ATP, phytic acid), Fe-bound P (phosphate adsorbed to ferrihydrite, phosphate adsorbed to goethite), Al-bound P (phosphate adsorbed to $Al(OH)_3$, $AlPO_4$), and Ca-bound P (hydroxyapatite, $CaHPO_4$). Standard spectra reported by Werner and Prietzel[44] and Gustafsson et al.[45] were shifted by −2.0 eV to align with comparable standard spectra collected at CLS (i.e., phosphate adsorbed to goethite and $CaHPO_4$). Best fits were determined using the same criteria reported for Fe speciation. Standard spectra that generated negative contributions were removed from fits for individual samples by rerunning the linear combination fitting without that standard included as a contributor. Calcium speciation was investigated using linear combination fits to $\mu(E)$ from −20 to +30 eV around the Ca K-edge. Standards used in the fits included spectra from $CaHPO_4$ and hydroxyapatite powders collected during our beamtime as well as spectra for apatite, calcite, Ca-pectate, Ca-acetylacetonate, kaolin, and smectite previously collected at SXRMB by the beamline scientists. Summaries of the linear combination fit for all Fe, P, and Ca spectra are provided in Tables S3−S6. The mass proportions of different compounds were calculated as the fraction of that compound determined by linear combination fits multiplied by the total concentration of that element in the sample.

Statistical Analysis. All statistical analyses were performed using R Statistical Software (v4.3.0).[46] Statistical comparisons between sample groups reported in the text were calculated using two-sample t-tests with a confidence interval of 95%. When p-values were lower than 0.05 (i.e., $p < 0.05$), differences in the numerical results were considered statistically significant. All calculated results with uncertainties presented in the text are reported as mean ± SEM. All data figures were plotted using the *ggplot2* R package (v3.4.3).[47]

RESULTS AND DISCUSSION

Bulk Element Concentrations. The bulk Fe and organic content of hillslope soils were similar across topographic positions (i.e., upland, slope, lowland) and vertically between surface and subsurface O horizons (Figure 2a,b). The exception was the subsurface O horizon in the lowland acidic tundra, which was substantially enriched in Fe (~115 g Fe·kg $soil^{-1}$) relative to upland and nonacidic soils (Fe < 35 g Fe·kg $soil^{-1}$). Aluminum (Al) and Si concentrations were higher in subsurface O horizons than surface O horizons (~155% enrichment of Al; ~74% enrichment of Si; see Table S3), which presumably reflected higher mineral content in the subsurface O horizons due to mixing with the underlying mineral soil. In addition, the total amount of base cations was significantly higher in the nonacidic hillslope (22.6 ± 0.6 g·kg $soil^{-1}$) than in the acidic hillslope (13.0 ± 1.2 g·kg $soil^{-1}$; Table S3).

Biogenic Fe mats exhibited geochemical properties that were distinct from tundra hillslope soils and from pond sediments in mining-disturbed areas (Figure 2). Biogenic Fe mats contained higher concentrations of Fe (219 ± 18 g Fe·kg^{-1}) and organic material (53.6 ± 1.3%) relative to the mining-disturbed ponds (35 ± 1 g Fe·kg^{-1}, 6.7 ± 0.9% organic material), but had lower amounts of base cations (i.e., Ca, Mg, Na, K), silicon (Si), and other presumably bedrock-derived elements (Table S3). Notably, Fe was enriched by at least 280% in pond sediments supporting biogenic Fe mats relative to pond sediments in mining-disturbed areas. There was a wider range of Fe concentrations in biogenic Fe mats formed at pond sediment−water interfaces (134−292 g Fe·kg^{-1}) compared to those associated with submerged plant material (229−255 g Fe·kg^{-1}; Figure 2b), but all other geochemical properties between the two groups of biogenic Fe mats were similar.

Iron Oxidation State and Speciation. Iron K-edge XAS was used to identify and compare the average oxidation state and speciation of Fe in biogenic Fe mats to the mining-disturbed ponds, tundra hillslope soils, and retrogressive thaw slumps (RTS). All samples contained mostly Fe(III) (50−

https://doi.org/10.1021/acs.est.3c09072
Environ. Sci. Technol. XXXX, XXX, XXX−XXX

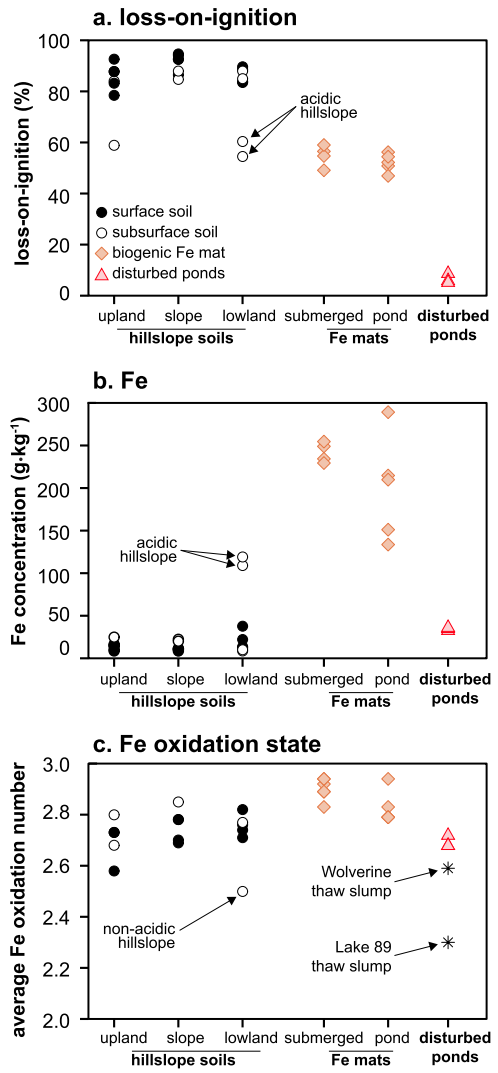

Figure 2. (a) Loss-on-ignition (LOI, %), (b) total Fe concentrations (g Fe·kg^{-1}), and (c) average Fe oxidation state of materials collected from hillslope soils, biogenic Fe mats, and pond sediments in areas disturbed by mining. (c) Average iron oxidation states were calculated from linear combination fits to Fe K-edge XANES spectra (Table S4). The stars in (c) denote samples from permafrost thaw slump mud slurries. LOI and total Fe concentrations were not evaluated for the thaw slump samples.

95%), except for the Lake 89 RTS which contained 70% Fe(II) (Figure 2c, Table S4). The average oxidation state of Fe in hillslope soils was similar across hillslope positions (2.73 ± 0.02). There was a relatively low Fe oxidation state in the subsurface O horizon at the lowland position of the nonacidic hillslope that could indicate either more reducing conditions or the presence of Fe(II)-bearing silicates. Iron oxidation state was significantly higher ($p < 0.05$) in biogenic Fe mats from undisturbed wet sedge habitats (2.87 ± 0.04) than in hillslope soils (2.73 ± 0.02) or mining-disturbed pond sediments (2.69 ± 0.01).

In hillslope soils, concentrations and proportions of SRO Fe(III) oxyhydroxides were highest in lowlands, largely driven by Fe accumulations in subsurface horizons of the acidic tundra (Figure 3a). Organic-bound Fe(III) was proportionally highest in upland soils, consistent with previous studies showing that organic-bound Fe(III) may be more abundant than Fe(III) oxyhydroxides in acidic soils.[9,32,34,48] Fe-bearing clays increased slightly moving down the hillslope, but the differences between each hillslope position were not significant (i.e., $p > 0.05$). This may indicate that chemical weathering processes that cause the transport and/or formation of Fe-bearing clay minerals had a lesser effect on Fe speciation than redox-driven processes that result in the formation of SRO Fe phases and Fe(III)-organic matter complexes.

Biogenic Fe mats were dominated by short-range ordered (SRO) Fe(III) oxyhydroxides, whereas mining-disturbed ponds contained mostly organic-bound Fe(III) and Fe(II)-bearing clays (Figure 3a, Table S5). Correspondingly, the average mass concentration of SRO Fe was significantly higher ($p < 0.05$) in biogenic Fe mats (135 ± 16 g·kg^{-1}) than in the mining-disturbed ponds (2.5 ± 1.3 g·kg^{-1}). These results align with the reported dominance of SRO Fe(III) oxyhydroxides in biogenic Fe mats.[24,49] In addition, SRO Fe phases were more prevalent in biogenic mats associated with submerged vegetation (73 ± 8%) than Fe mats at pond sediment-water interfaces (47 ± 11%), whereas the pond biogenic Fe mats had higher amounts of organic-bound Fe(III). The Lake 89 thaw slump sample contained mostly Fe(II)-bearing clays (45%) with 31% SRO Fe(III) oxyhydroxides and 9% organic-bound Fe(III), whereas the Wolverine thaw slump contained 52% SRO Fe(III) oxyhydroxides, 17% Fe(II)-bearing clays, and 17% organic-bound Fe(III) (Table S5).

Crystalline Fe(III) oxides, organic-bound Fe(II), and Fe-phosphate minerals comprised a relatively small proportion (<15%) of total Fe (Table S5). This suggests that the microbial dissolution and formation of SRO Fe phases may outcompete the ripening of SRO into crystalline Fe (oxyhydr)-oxides in these dynamic redox systems. In addition, the greater abundance of organic-bound Fe(III) and Fe(III) (oxyhydr)-oxides relative to crystalline Fe(III) oxides and organic-bound Fe(II) may indicate that all sampling locations experience consistent or transiently oxic conditions. Nutrient limitation may be another factor influencing Fe speciation. For example, although Fe (oxyhydr)oxides can bind large quantities of phosphate, tundra soils often contain low amounts of available phosphate which could limit the formation of Fe-phosphate precipitates (e.g., vivianite).[5−8]

From these results, we infer that Fe is mobilized and transformed across the transition from tussock uplands to wet sedge lowlands and into ponds and streams. The progressive increase in Fe, and in particular SRO Fe(III) oxyhydroxides, down the hillslope toward the lowlands is a key signature of increasing activity of Fe-oxidizing microorganisms, resulting in the formation of biogenic Fe mats which are primarily comprised of SRO Fe phases (Figure 2).[25,28]

Calcium Speciation. Biogenic Fe mats associated with submerged vegetation contained primarily organic-bound Ca (43 ± 11%) followed by Ca^{2+} associated with clay minerals (31 ± 6%) and Ca phosphates (23 ± 4%). Biogenic Fe mats formed at pond sediment−water interfaces had a higher proportion of organic-bound Ca (57 ± 10%) and slightly more Ca phosphates (16 ± 1%) than Ca^{2+} associated with clays (14 ± 3%). The disturbed pond sediments exhibited the lowest proportion of organic-bound Ca (38 ± 6%) and similar amounts of Ca phosphates (32 ± 3%) and Ca^{2+} associated with clays (27 ± 4%). Calcium carbonate was a minor component in all collected samples (<10%). Overall, there was a significant enrichment of Ca phosphates in disturbed pond sediments relative to pond sediments supporting biogenic Fe

https://doi.org/10.1021/acs.est.3c09072
Environ. Sci. Technol. XXXX, XXX, XXX−XXX

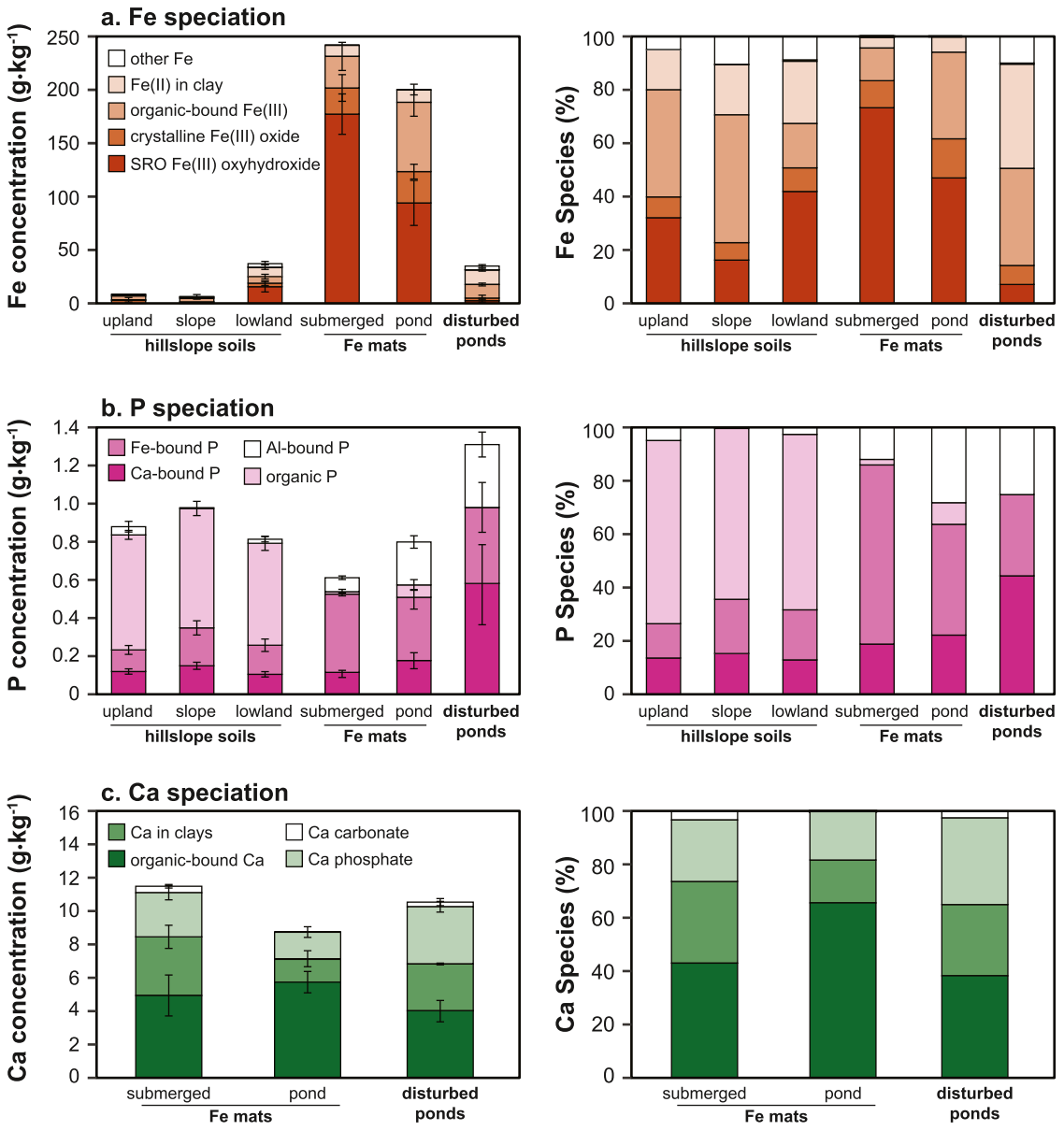

Figure 3. (left panels) Mass concentrations (g·kg^{-1} soil) and (right panels) relative proportions of Fe, P, and Ca soil minerals in hillslope soils, biogenic Fe mats, and pond sediments in areas disturbed by mining. Error bars represent standard error of the mean. Element speciation was calculated from linear combination fits to XAS spectra. The legend in the left panel also applies to the right panel. (a) Iron speciation was determined from K-edge EXAFS analysis. The "other Fe" category includes vivianite, phosphate adsorbed to Fe(III), and oxalate-bound Fe(II). (b, c) P and Ca speciation were determined from K-edge XANES analysis. Data shown for each hillslope soil includes combined results for each hillslope transect (acidic and nonacidic) and O horizons (surface and subsurface). No Ca speciation data were collected for hillslope soils.

mats (75% enrichment, $p < 0.05$), indicating a shift toward more Ca−P associations in mining-disturbed habitats.

Phosphorus Speciation. Hillslope soils contained high proportions of organic P species (66 ± 3%) with relatively small amounts of Ca- and Fe-bound P. There were no significant trends in P species along the hillslope toposequence. Biogenic Fe mats contained mostly phosphate bound to Fe (oxyhydr)oxides and had significantly higher ($p < 0.05$) proportions of Fe-bound P than the mining-disturbed ponds and hillslope soils (Figures 3b and S3 and S4, Table S6). Aluminum-bound P was higher in biogenic Fe mats formed at pond sediment−water interfaces (28 ± 4%) than those associated with submerged plant material (12 ± 0.3%). All biogenic Fe mats had low amounts of organic P (mean 6 ± 2%). The sediments in mining-disturbed ponds were dominated by Ca−P phases (e.g., $CaHPO_4$, (hydroxy)apatite) and contained similar proportions of Al- and Fe-bound P (~25−30%). No organic P species were detected in any of the disturbed sites.

These results indicate that landscape position may determine the dominant processes driving phosphate bioavailability (Figure 4). In upland soils, dephosphorylation of organic matter by plant and microbial phosphatase enzymes may release phosphate into solution where it can be removed by microbial and plant uptake.[7] In saturated lowland soils, Fe mats may immobilize phosphate cleaved from organic matter and/or sequester phosphate as it is transported downslope.[50] In addition, organic P, which comprised 35−86% of total P in hillslope soils, may form strong outer-sphere complexes with mineral surfaces.[51−53] At the pond sediment−water interface

https://doi.org/10.1021/acs.est.3c09072
Environ. Sci. Technol. XXXX, XXX, XXX−XXX

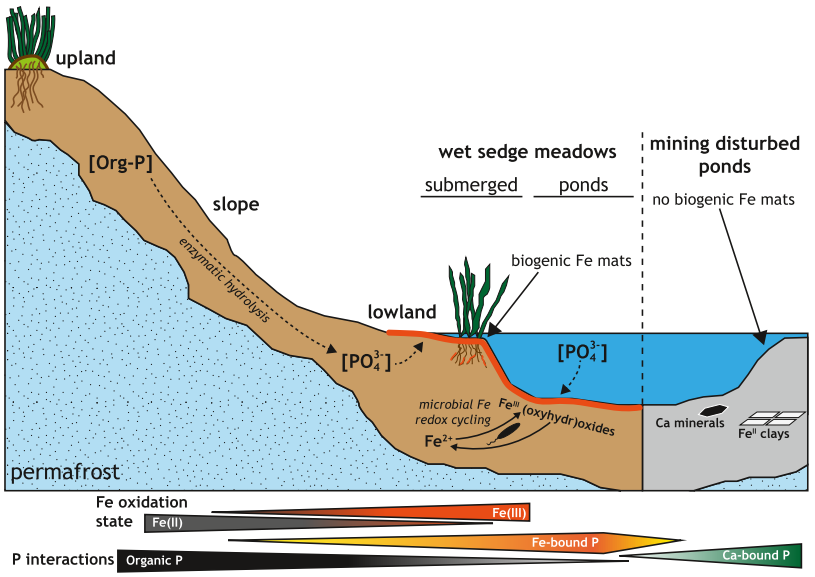

Figure 4. Conceptual representation of the differences in P interactions between hillslope soils, biogenic Fe mats, and mining-disturbed pond sediments. The proportion of Fe(III) increased down the hillslope toposequence and into the undisturbed wet sedge meadows which supported biogenic Fe mats. Mining-disturbed ponds were associated with a loss of biogenic Fe mats. The dominant P species shifted from organic P in hillslopes to Fe-bound P in biogenic Fe mats and Ca-bound P in disturbed pond sediments.

(i.e., pond mats), Fe mats may bind P leaching from soil water, dissolved in the water column, or released from the reductive dissolution of other Fe(III) phases in the sediments during periods of anoxia.[54,55] Our data suggest that SRO Fe(III) oxyhydroxides dominate phosphate sorption at redox interfaces in the wet sedge tundra (Figure 3a). Indeed, the Fe mats in our study contained the highest overall concentrations of Fe-bound P (0.37 ± 0.04 g·kg^{-1}; Figure 3, Table S5) despite having the lowest average concentration of total P (0.70 ± 0.07 g·kg^{-1}; Table S3). These results are consistent with previous observations that demonstrate a strong correlation between the concentration of low crystallinity Fe oxide phases with both the phosphate sorption capacity and concentrations of labile P in boreal and tundra systems.[9] Furthermore, soils throughout the Toolik region exhibit a negative relationship between oxalate-extractable Fe and Mehlich-III P (Figure 5),[56] indicating that P bioavailability decreases where Fe(III) oxyhydroxides accumulate and supporting our assertion that Fe oxyhydroxides that form at redox interfaces are critical controls on P solubility in arctic tundra.

Environmental Implications. In this study, we identified differences in the speciation and associations of P with soil minerals across undisturbed and disturbed Arctic tundra ecosystems. Most notably, we observed a shift from P associations with Fe (oxyhydr)oxides that comprise biogenic Fe mats in undisturbed wet sedge meadows to interactions with Ca minerals in areas impacted by physical disturbances (Figure 3). Considering that frequent redox cycling supports the formation and dissolution of Fe(III) (oxyhydr)-oxides,[25,28,57] we infer that biogenic Fe mats represent important redox interfaces in wet sedge tundra that may influence P bioavailability primarily via adsorption of phosphate to SRO Fe(III) oxyhydroxides (Figure 4). As such, processes that alter the geochemical and hydrologic characteristics of tundra systems (e.g., climate warming,[58−60] mineral extraction,[24,61] land cover change[62]) may affect the spatial distribution of these important redox interfaces and directly impact the accumulation of Fe (oxyhydr)oxides and

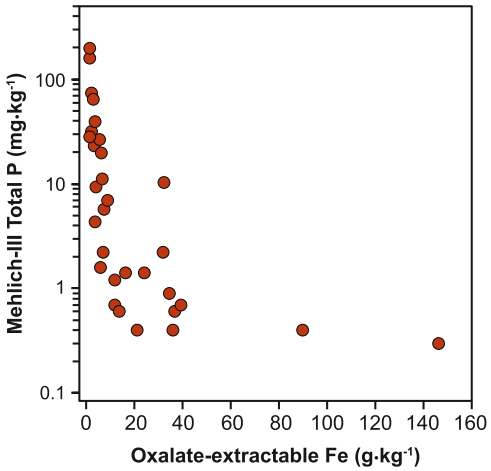

Figure 5. Mehlich-III extractable soil P and oxalate-extractable soil Fe were measured during the distributed initial characterization of 18 sites from around Toolik Field Station (TOOL). The data were reported by the National Ecological Observatory Network (NEON).[37] The represented soil samples were collected from organic horizons in the top 1 m of the soil profile in August 2018. Oxalate-extractable Fe includes organically complexed and non- and semicrystalline Fe in addition to magnetite (Fe_3O_4) and minor amounts of crystalline Fe and trioctahedral Fe phyllosilicates.[38−40] Mehlich-III P includes orthophosphate extractable by acetic acid and fluoride compounds and is an estimate of total plant available P.

regulate P bioavailability to tundra plants and microorganisms in a warming Arctic climate.

Landscape disturbances were associated with an absence of biogenic Fe mats and a shift toward more P interactions with Ca minerals and Fe(II)-bearing clays (Figure 3; Tables S5−S7).[61] As both chronic and episodic disturbances are becoming increasingly common across the Alaskan Arctic, we contend that this could limit potential P retention at wet sedge redox interfaces by inhibiting microbial Fe cycling and inducing a shift from primarily redox-controlled P interactions to those

https://doi.org/10.1021/acs.est.3c09072
Environ. Sci. Technol. XXXX, XXX, XXX−XXX

that are more susceptible to changes in pH. For example, Fe(II) clays and Ca minerals are effective sorbents for phosphate and organic P[17,63−65] but are susceptible to dissolution and P release under acidic conditions (pH < ∼5).[22,23] Moreover, gravel mining may increase soil alkalinity and either enhance or inhibit P retention by promoting the coprecipitation of Ca phosphate species or raising the pH above the point of zero charge of soil minerals, respectively.[66−68] A further compounding factor is that gravel mining in our study area occurred approximately 50 years ago, yet biogenic Fe mats have never reestablished. This observation provides a striking example of the long-term impacts of mining disturbance on microbial Fe cycling, and in turn, the ability of wet sedge redox interfaces to recover and mediate P bioavailability in postmining landscapes.

The retrogressive thaw slumps develop as a consequence of accelerated permafrost thaw that is becoming increasingly common under a warming Arctic climate.[69−73] In contrast to the physical removal or organic soil horizons during mining, the high proportion of Fe(II) in RTS slurries (up to 70%) relative to ponds in mining-disturbed areas (28−32%) and the biogenic Fe mats (6−21%; Figure 2d) reflects the mixing of organic and mineral horizons during soil collapse that can solubilize soil minerals previously trapped in permafrost and export considerable amounts of C and bioavailable P into aquatic systems.[74,75] However, the proportion of Fe(III) and Fe(oxyhydr)oxides in RTS slurries appears to increase with RTS age, which may indicate that some microbial Fe cycling has been reestablished following initial soil collapse. It is possible that although RTS can significantly alter soil P interactions, the redox interfaces within the affected landscape may reestablish their function as mediators of P mobility over much shorter time scales than areas impacted by gravel mining.

The time scales of P retention by SRO Fe oxyhydroxides at redox interfaces remain unclear. Transient anoxia driven by fluctuating water tables promotes reductive dissolution of SRO Fe phases to release phosphate, thus providing a source of bioavailable P that may be resorbed as Fe(III) oxyhydroxides reprecipitate under oxic conditions. Under a transition to persistently anoxic conditions (e.g., soil flooding from increased Arctic precipitation[76] and thermokarst development[77]), Fe reduction may release phosphate into P-limited aquatic systems and fuel primary production, thus partially offsetting C losses linked to permafrost thaw.[1,2,5,7] Repeated redox cycling may facilitate the transformation of SRO Fe oxyhydroxides into crystalline Fe phases[78] which confer a lower phosphate sorption capacity, but are less thermodynamically favorable to Fe-reducing bacteria[79] and could immobilize P over longer time scales.[9,78,79] Continued activity of Fe-oxidizing bacteria in wet sedge meadow habitats could counteract this mineral aging process.[14,80] and perpetuate the prevalence of SRO Fe(III) oxyhydroxides that may be long-term P sinks. These processes may be severely disrupted by future climate- and human-induced disturbances that inhibit microbial Fe cycling at redox interfaces and shift the quantity and composition of P associations with soil minerals. In addition, enhanced evapotranspiration and thawing permafrost may create deeper flow paths that limit potential interactions of soil P with Fe mats.[81] Thus, our study indicates that redox interfaces in wet sedge meadows form important barriers regulating P transport into nutrient-limited aquatic systems but are sensitive to disturbance.

■ ASSOCIATED CONTENT

Supporting Information

The Supporting Information is available free of charge at https://pubs.acs.org/doi/10.1021/acs.est.3c09072

Additional details on sampling locations, bulk element concentrations, and figures of XAS spectra; complete processed EXAFS spectra and normalized XANES spectra of all samples included in the manuscript and reference standards (PDF)

Normalized P and Ca XANES spectra with linear combination fits (XLSX)

■ AUTHOR INFORMATION

Corresponding Author

Elizabeth M. Herndon − *Environmental Sciences Division, Oak Ridge National Laboratory, Oak Ridge, Tennessee 37831, United States; Department of Earth and Planetary Sciences, University of Tennessee, Knoxville, Tennessee 37996, United States;* orcid.org/0000-0002-9194-5493; Email: herndonem@ornl.gov

Authors

Matthew John Berens − *Environmental Sciences Division, Oak Ridge National Laboratory, Oak Ridge, Tennessee 37831, United States;* orcid.org/0000-0002-4228-1133

Alexander Bryce Michaud − *School of Earth Sciences, Ohio State University, Columbus, Ohio 43210, United States; Byrd Polar and Climate Research Center, Ohio State University, Columbus, Ohio 43210, United States; Bigelow Laboratory for Ocean Sciences, East Boothbay, Maine 02543, United States*

Erin VanderJeugdt − *Department of Biological Sciences, Kent State University, Kent, Ohio 44240, United States*

Imtiaz Miah − *Department of Environmental Sciences, University of Toledo, Toledo, Ohio 43606, United States; Department of Agricultural Chemistry, Sylhet Agricultural University, Sylhet 3100, Bangladesh*

Frederick W. Sutor − *Rubenstein School of Environment and Natural Resources, University of Vermont, Burlington, Vermont 05405, United States*

David Emerson − *School of Earth Sciences, Ohio State University, Columbus, Ohio 43210, United States*

William B. Bowden − *Rubenstein School of Environment and Natural Resources, University of Vermont, Burlington, Vermont 05405, United States*

Lauren Kinsman-Costello − *Department of Biological Sciences, Kent State University, Kent, Ohio 44240, United States*

Michael N. Weintraub − *Department of Environmental Sciences, University of Toledo, Toledo, Ohio 43606, United States;* orcid.org/0000-0002-9623-2855

Complete contact information is available at: https://pubs.acs.org/10.1021/acs.est.3c09072

Notes

The authors declare no competing financial interest.

the published form of this manuscript, or allow others to do so, for US government purposes. DOE will provide public access to these results of federally sponsored research in accordance with the DOE Public Access Plan (https://www.energy.gov/doe-public-access-plan).

■ ACKNOWLEDGMENTS

This work was funded by the National Science Foundation grants OPP 2006194 and EAR 1609027 awarded to E.M.H. and L.K.-C., DEB 1754358 awarded to D.E., and DEB 1754379 and DEB 1637459 awarded to W.B.B. M.B. was supported by an award made to E.M.H. through the Department of Energy Office of Science Early Career Research Program. This research used resources of the Advanced Photon Source, an Office of Science User Facility operated for the U.S. Department of Energy (DOE) Office of Science by Argonne National Laboratory and was supported by the U.S. DOE under Contract No. DE-AC02-06CH11357, and the Canadian Light Source and its funding partners. XAS spectra were collected at APS beamline 9-BM via remote user access with assistance from Tiangping Wu. Part or all of the research described in this paper was performed at the Canadian Light Source, a national research facility of the University of Saskatchewan, which is supported by the Canada Foundation for Innovation (CFI), the Natural Sciences and Engineering Research Council (NSERC), the National Research Council (NRC), the Canadian Institutes of Health Research (CIHR), the Government of Saskatchewan, and the University of Saskatchewan. XAS spectra were collected at CLS beamline SXRMB by E.M.H. with assistance from Yongfeng Hu and Mohsen Shakouri. The authors would also like to acknowledge Maximilian Barczok for assistance with sample preparation and analysis at SXRMB.

■ REFERENCES

(1) Schuur, E. A. G.; Vogel, J. G.; Crummer, K. G.; Lee, H.; Sickman, J. O.; Osterkamp, T. E. The Effect of Permafrost Thaw on Old Carbon Release and Net Carbon Exchange from Tundra. *Nature* **2009**, *459* (7246), 556−559.

(2) Koven, C. D.; Ringeval, B.; Friedlingstein, P.; Ciais, P.; Cadule, P.; Khvorostyanov, D.; Krinner, G.; Tarnocai, C. Permafrost Carbon-Climate Feedbacks Accelerate Global Warming. *Proc. Natl. Acad. Sci. U.S.A.* **2011**, *108* (36), 14769−14774.

(3) McGuire, A. D.; Genet, H.; Lyu, Z.; Pastick, N.; Stackpoole, S.; Birdsey, R.; D'Amore, D.; He, Y.; Rupp, T. S.; Striegl, R.; Wylie, B. K.; Zhou, X.; Zhuang, Q.; Zhu, Z. Assessing Historical and Projected Carbon Balance of Alaska: A Synthesis of Results and Policy/Management Implications. *Ecol. Appl.* **2018**, *28* (6), 1396−1412.

(4) Wieder, W. R.; Cleveland, C. C.; Smith, W. K.; Todd-Brown, K. Future Productivity and Carbon Storage Limited by Terrestrial Nutrient Availability. *Nat. Geosci.* **2015**, *8* (6), 441−444.

(5) Chapin, F. S.; Barsdate, R. J.; Barèl, D.; Barel, D. Phosphorus Cycling in Alaskan Coastal Tundra: A Hypothesis for the Regulation of Nutrient Cycling. *Oikos* **1978**, *31* (2), 189−199.

(6) Walbridge, M. R.; Navaratnam, J. A. Phosphorous in Boreal Peatlands. In *Boreal Peatland Ecosystems*; Wieder, R. K.; Vitt, D. H., Eds.; Springer: Berlin, Heidelberg, 2006; pp 231−258.

(7) Weintraub, M. N. Biological Phosphorus Cycling in Arctic and Alpine Soils. In *Phosphorus in Action; Soil Biology*; Springer: Berlin, Heidelberg, 2011; Vol. *26*, pp 295−316.

(8) Shaw, A. N.; Cleveland, C. C. The Effects of Temperature on Soil Phosphorus Availability and Phosphatase Enzyme Activities: A Cross-Ecosystem Study from the Tropics to the Arctic. *Biogeochemistry* **2020**, *151* (2), 113−125.

(9) Herndon, E. M.; Kinsman-Costello, L.; Duroe, K. A.; Mills, J.; Kane, E. S.; Sebestyen, S. D.; Thompson, A. A.; Wullschleger, S. D. Iron (Oxyhydr)Oxides Serve as Phosphate Traps in Tundra and Boreal Peat Soils. *J. Geophys. Res.: Biogeosci.* **2019**, *124* (2), 227−246.

(10) Rentz, J. A.; Turner, I. P.; Ullman, J. L. Removal of Phosphorus from Solution Using Biogenic Iron Oxides. *Water Res.* **2009**, *43* (7), 2029−2035.

(11) Baken, S.; Salaets, P.; Desmet, N.; Seuntjens, P.; Vanlierde, E.; Smolders, E. Oxidation of Iron Causes Removal of Phosphorus and Arsenic from Streamwater in Groundwater-Fed Lowland Catchments. *Environ. Sci. Technol.* **2015**, *49* (5), 2886−2894.

(12) Bridgham, S. D.; Updegraff, K.; Pastor, J. Carbon, Nitrogen, and Phosphorus Mineralization in Northern Wetlands. *Ecology* **1998**, *79* (5), 1545−1561.

(13) Henderson, R.; Kabengi, N.; Mantripragada, N.; Cabrera, M.; Hassan, S.; Thompson, A. Anoxia-Induced Release of Colloid- and Nanoparticle-Bound Phosphorus in Grassland Soils. *Environ. Sci. Technol.* **2012**, *46* (21), 11727−11734.

(14) Roden, E. E. Fe(III) Oxide Reactivity Toward Biological versus Chemical Reduction. *Environ. Sci. Technol.* **2003**, *37* (7), 1319−1324.

(15) Tunesi, S.; Poggi, V.; Gessa, C. Phosphate Adsorption and Precipitation in Calcareous Soils: The Role of Calcium Ions in Solution and Carbonate Minerals. *Nutr. Cycling Agroecosyst.* **1999**, *53* (3), 219−227.

(16) Tanada, S.; Kabayama, M.; Kawasaki, N.; Sakiyama, T.; Nakamura, T.; Araki, M.; Tamura, T. Removal of Phosphate by Aluminum Oxide Hydroxide. *J. Colloid Interface Sci.* **2003**, *257* (1), 135−140.

(17) Gérard, F. Clay Minerals, Iron/Aluminum Oxides, and Their Contribution to Phosphate Sorption in Soils — A Myth Revisited. *Geoderma* **2016**, *262*, 213−226.

(18) Prietzel, J.; Klysubun, W.; Hurtarte, L. C. C. The Fate of Calcium in Temperate Forest Soils: A Ca K-Edge XANES Study. *Biogeochemistry* **2021**, *152* (2), 195−222.

(19) Turner, B. L.; Papházy, M. J.; Haygarth, P. M.; Mckelvie, I. D. Inositol Phosphates in the Environment. *Philos. Trans. R. Soc., B* **2002**, *357* (1420), 449−469.

(20) Stewart, J. W. B.; Tiessen, H. Dynamics of Soil Organic Phosphorus. *Biogeochemistry* **1987**, *4* (1), 41−60.

(21) Prietzel, J.; Klysubun, W.; Werner, F. Speciation of Phosphorus in Temperate Zone Forest Soils as Assessed by Combined Wet-Chemical Fractionation and XANES Spectroscopy. *J. Plant Nutr. Soil Sci.* **2016**, *179* (2), 168−185.

(22) Hamer, M.; Graham, R. C.; Amrhein, C.; Bozhilov, K. N. Dissolution of Ripidolite (Mg, Fe-Chlorite) in Organic and Inorganic Acid Solutions. *Soil Sci. Soc. Am. J.* **2003**, *67* (2), 654−661.

(23) Brydon, J. E.; Ross, G. J. Stability of Chlorite in Dilute Acid Solutions. *Soil Sci. Soc. Am. J.* **1966**, *30* (6), 740−744.

(24) Michaud, A. B.; Massé, R. O.; Emerson, D. Microbial Iron Cycling Is Prevalent in Water-Logged Alaskan Arctic Tundra Habitats, but Sensitive to Disturbance. *FEMS Microbiol. Ecol.* **2023**, *99* (3), No. fiad013, DOI: 10.1093/femsec/fiad013.

(25) Emerson, D.; Fleming, E. J.; McBeth, J. M. Iron-Oxidizing Bacteria: An Environmental and Genomic Perspective. *Annu. Rev. Microbiol.* **2010**, *64* (1), 561−583.

(26) Vigliaturo, R.; Marengo, A.; Bittarello, E.; Perez-Rodriguez, I.; Drazic, G.; Giere, R. Micro- and Nano-Scale Mineralogical Characterization of Fe(II)-Oxidizing Bacterial Stalks. *Geobiology* **2020**, *18* (5), 606−618.

(27) Patzner, M. S.; Logan, M.; Mckenna, A. M.; Young, R. B.; Zhou, Z.; Joss, H.; Mueller, C. W.; Hoeschen, C.; Scholten, T.; Straub, D.; Kleindienst, S.; Borch, T.; Kappler, A.; Bryce, C. Microbial Iron Cycling during Palsa Hillslope Collapse Promotes Greenhouse Gas Emissions before Complete Permafrost Thaw. *Commun. Earth Environ* **2022**, *3* (1), No. 76, DOI: 10.1038/s43247-022-00407-8.

(28) Emerson, D.; Scott, J. J.; Benes, J.; Bowden, W. B. Microbial Iron Oxidation in the Arctic Tundra and Its Implications for Biogeochemical Cycling. *Appl. Environ. Microbiol.* **2015**, *81* (23), 8066.

https://doi.org/10.1021/acs.est.3c09072
Environ. Sci. Technol. XXXX, XXX, XXX−XXX

(29) Chan, C. S.; Fakra, S. C.; Edwards, D. C.; Emerson, D.; Banfield, J. F. Iron Oxyhydroxide Mineralization on Microbial Extracellular Polysaccharides. *Geochim. Cosmochim. Acta* **2009**, *73* (13), 3807−3818.
(30) Patzner, M. S.; Mueller, C. W.; Malusova, M.; Baur, M.; Nikeleit, V.; Scholten, T.; Hoeschen, C.; Byrne, J. M.; Borch, T.; Kappler, A.; Bryce, C. Iron Mineral Dissolution Releases Iron and Associated Organic Carbon during Permafrost Thaw. *Nat. Commun.* **2020**, *11* (1), No. 6329, DOI: 10.1038/s41467-020-20102-6.
(31) Patzner, M. S.; Kainz, N.; Lundin, E.; Barczok, M.; Smith, C.; Herndon, E.; Kinsman-Costello, L.; Fischer, S.; Straub, D.; Kleindienst, S.; Kappler, A.; Bryce, C. Seasonal Fluctuations in Iron Cycling in Thawing Permafrost Peatlands. *Environ. Sci. Technol.* **2022**, *56* (7), 4620−4631.
(32) Shaver, G. R.; Laundre, J. A.; Bret-Harte, M. S.; Iii, F. S. C.; Mercado-Díaz, J. A.; Giblin, A. E.; Gough, L.; Gould, W. A.; Hobbie, S. E.; Mack, M. C.; Moore, J. C.; Nadelhoffer, K. J.; Rastetter, E. B.; Schimel, J. P. Terrestrial Ecosystems at Toolik Lake, Alaska. In *Alaska's Changing Arctic: Ecological Consequences for Tundra, Streams, and Lakes*; Hobbie, J. E.; Kling, G. W., Eds.; Oxford University Press: Oxford, New York, 2014; Vol. *2014*, pp 90−142.
(33) Whittinghill, K. A.; Hobbie, S. E. Effects of Landscape Age on Soil Organic Matter Processing in Northern Alaska. *Soil Sci. Soc. Am. J.* **2011**, *75* (3), 907−917.
(34) Giblin, A. E.; Nadelhoffer, K. J.; Shaver, G. R.; Laundre, J. A.; McKerrow, A. J. Biogeochemical Diversity Along a Riverside Toposequence in Arctic Alaska. *Ecol. Monogr.* **1991**, *61* (4), 415−435.
(35) Boelman, N. T.; Stieglitz, M.; Rueth, H. M.; Sommerkorn, M.; Griffin, K. L.; Shaver, G. R.; Gamon, J. A. Response of NDVI, Biomass, and Ecosystem Gas Exchange to Long-Term Warming and Fertilization in Wet Sedge Tundra. *Oecologia* **2003**, *135* (3), 414−421.
(36) Arp, C. D.; Whitman, M. S.; Jones, B. M.; Grosse, G.; Gaglioti, B. V.; Heim, K. C. Distribution and Biophysical Processes of Beaded Streams in Arctic Permafrost Landscapes. *Biogeosciences* **2015**, *12* (1), 29−47.
(37) National Ecological Observatory Network (NEON). *Soil Physical and Chemical Properties, Distributed Initial Characterization (DP1.10047.001)*, 2024, DOI: 10.48443/R517-KG13.
(38) Parfitt, R. L.; Childs, C. W. Estimation of Forms of Fe and Al: A Review, and Analysis of Contrasting Soils by Dissolution and Moessbauer Methods. *Aust. J. Soil Res.* **1988**, *26* (1), 121−144.
(39) Ross, G. J.; Wang, C. Extractable Al, Fe, Mn, and Si. In *Soil Sampling and Methods of Analysis*; Lewis Publishers: Boca Raton, FL, 1993; pp 239−246.
(40) Shang, C.; Zelazny, L. W. Selective Dissolution Techniques for Mineral Analysis of Soils and Sediments. In *Methods of Soil Analysis Part 5—Mineralogical Methods*; John Wiley & Sons, Ltd., 2008; pp 33−80.
(41) Mehlich, A. Mehlich 3 Soil Test Extractant: A Modification of Mehlic 2 Extractant. *Commun. Soil Plant Anal.* **1984**, *15*, 1409−1416, DOI: 10.1080/00103628409367568.
(42) Ravel, B.; Newville, M. ATHENA, ARTEMIS, HEPHAESTUS: Data Analysis for X-Ray Absorption Spectroscopy Using It IFEFFIT. *J. Synchrotron Radiat.* **2005**, *12* (4), 537−541.
(43) O'Day, P. A.; Rivera, N.; Root, R.; Carroll, S. A. X-Ray Absorption Spectroscopic Study of Fe Reference Compounds for the Analysis of Natural Sediments. *Am. Mineral.* **2004**, *89* (4), 572−585.
(44) Werner, F.; Prietzel, J. Standard Protocol and Quality Assessment of Soil Phosphorus Speciation by P *K*-Edge XANES Spectroscopy. *Environ. Sci. Technol.* **2015**, *49* (17), 10521−10528.
(45) Gustafsson, J. P.; Braun, S.; Tuyishime, J. R. M.; Adediran, G. A.; Warrinnier, R.; Hesterberg, D. A Probabilistic Approach to Phosphorus Speciation of Soils Using P K-Edge XANES Spectroscopy with Linear Combination Fitting. *Soil Syst.* **2020**, *4* (2), No. 26, DOI: 10.3390/soilsystems4020026.
(46) R Core Team. R: A Language and Environment for Statistical Computing, 2023. https://www.R-project.org/.
(47) Wickham, H. *Ggplot2: Elegant Graphics for Data Analysis*; Springer-Verlag: New York, 2016.
(48) Karlsson, T.; Persson, P.; Skyllberg, U.; Mörth, C.-M.; Giesler, R. Characterization of Iron(III) in Organic Soils Using Extended X-Ray Absorption Fine Structure Spectroscopy. *Environ. Sci. Technol.* **2008**, *42* (15), 5449−5454.
(49) Mitsunobu, S.; Shiraishi, F.; Makita, H.; Orcutt, B. N.; Kikuchi, S.; Jorgensen, B. B.; Takahashi, Y. Bacteriogenic Fe(III) (Oxyhydr)-Oxides Characterized by Synchrotron Microprobe Coupled with Spatially Resolved Phylogenetic Analysis. *Environ. Sci. Technol.* **2012**, *46* (6), 3304−3311.
(50) Zak, D.; Gelbrecht, J.; Steinberg, C. E. W. Phosphorus Retention at the Redox Interface of Peatlands Adjacent to Surface Waters in Northeast Germany. *Biogeochemistry* **2004**, *70* (3), 357−368.
(51) Yan, Y.; Li, W.; Yang, J.; Zheng, A.; Liu, F.; Feng, X.; Sparks, D. L. Mechanism of Myo-Inositol Hexakisphosphate Sorption on Amorphous Aluminum Hydroxide: Spectroscopic Evidence for Rapid Surface Precipitation. *Environ. Sci. Technol.* **2014**, *48* (12), 6735−6742.
(52) Gerke, J. Humic (Organic Matter)-Al(Fe)-Phosphate Complexes: An Underestimated Phosphate Form in Soils and Source of Plant-Available Phosphate. *Soil Sci.* **2010**, *175* (9), 417 DOI: 10.1097/SS.0b013e3181f1b4dd.
(53) Hayes, J. E.; Simpson, R. J.; Richardson, A. E. The Growth and Phosphorus Utilisation of Plants in Sterile Media When Supplied with Inositol Hexaphosphate, Glucose 1-Phosphate or Inorganic Phosphate. *Plant Soil* **2000**, *220* (1), 165−174.
(54) MacIntyre, S.; Sickman, J. O.; Goldthwait, S. A.; Kling, G. W. Physical Pathways of Nutrient Supply in a Small, Ultraoligotrophic Arctic Lake during Summer Stratification. *Limnol. Oceanogr.* **2006**, *51* (2), 1107−1124.
(55) Alam, M. S.; Barthod, B.; Li, J.; Liu, H.; Zastepa, A.; Liu, X.; Dittrich, M. Geochemical Controls on Internal Phosphorus Loading in Lake of the Woods. *Chem. Geol.* **2020**, *558*, No. 119873.
(56) National Ecological Observatory Network (NEON). *Soil Physical and Chemical Properties, Megapit (DP1.00096.001)*, 2024, DOI: 10.48443/S6ND-Q840.
(57) O'Connor, M. T.; Cardenas, M. B.; Neilson, B. T.; Nicholaides, K. D.; Kling, G. W. Active Layer Groundwater Flow: The Interrelated Effects of Stratigraphy, Thaw, and Topography. *Water Resour. Res.* **2019**, *55* (8), 6555−6576.
(58) Liu, Y.; Wang, P.; Elberling, B.; Westergaard-Nielsen, A. Drivers of Contemporary and Future Changes in Arctic Seasonal Transition Dates for a Tundra Site in Coastal Greenland. *Global Change Biol.* **2024**, *30* (1), No. e17118.
(59) Post, E.; Alley, R. B.; Christensen, T. R.; Macias-Fauria, M.; Forbes, B. C.; Gooseff, M. N.; Iler, A.; Kerby, J. T.; Laidre, K. L.; Mann, M. E.; Olofsson, J.; Stroeve, J. C.; Ulmer, F.; Virginia, R. A.; Wang, M. The Polar Regions in a 2°C Warmer World. *Sci. Adv.* **2019**, *5* (12), No. eaaw9883.
(60) Bintanja, R. The Impact of Arctic Warming on Increased Rainfall. *Sci. Rep.* **2018**, *8* (1), No. 16001.
(61) Auerbach, N. A.; Walker, M. D.; Walker, D. A. Effects of Roadside Disturbance on Substrate and Vegetation Properties in Arctic Tundra. *Ecol. Appl.* **1997**, *7* (1), 218−235.
(62) Wang, J. A.; Sulla-Menashe, D.; Woodcock, C. E.; Sonnentag, O.; Keeling, R. F.; Friedl, M. A. Extensive Land Cover Change across Arctic−Boreal Northwestern North America from Disturbance and Climate Forcing. *Global Change Biol.* **2020**, *26* (2), 807−822.
(63) Minamisawa, H.; Kojima, Y.; Aizawa, M. Adsorption of Inositol Phosphate on Hydroxyapatite Powder with High Specific Surface Area. *Materials* **2022**, *15* (6), No. 2176, DOI: 10.3390/ma15062176.
(64) Bar-Yosef, B.; Rosenberg, R.; Kafkafi, U.; Sposito, G. Phosphorus Adsorption by Kaolinite and Montmorillonite: I. Effect of Time, Ionic Strength, and pH. *Soil Sci. Soc. Am. J.* **1988**, *52* (6), 1580−1585.

(65) Edzwald, J. K.; Toensing, D. C.; Leung, M. C.-Y. Phosphate Adsorption Reactions with Clay Minerals. *Environ. Sci. Technol.* **1976**, *10* (5), 485−490.
(66) Essington, M. E. *Soil and Water Chemistry: An Integrative Approach*, 2nd ed.; CRC Press, 2015.
(67) Sindelar, H. R.; Brown, M. T.; Boyer, T. H. Effects of Natural Organic Matter on Calcium and Phosphorus Co-Precipitation. *Chemosphere* **2015**, *138*, 218−224.
(68) Diaz, O. A.; Reddy, K. R.; Moore, P. A. Solubility of Inorganic Phosphorus in Stream Water as Influenced by pH and Calcium Concentration. *Water Res.* **1994**, *28* (8), 1755−1763.
(69) Lantz, T. C.; Kokelj, S. V. Increasing Rates of Retrogressive Thaw Slump Activity in the Mackenzie Delta Region, N.W.T., Canada. *Geophys. Res. Lett.* **2008**, *35* (6), No. 1, DOI: 10.1029/2007GL032433.
(70) Lewkowicz, A. G.; Way, R. G. Extremes of Summer Climate Trigger Thousands of Thermokarst Landslides in a High Arctic Environment. *Nat. Commun.* **2019**, *10* (1), No. 1329.
(71) Swanson, D. K. Permafrost Thaw-Related Slope Failures in Alaska's Arctic National Parks, c. 1980−2019. *Permafr. Periglac. Process.* **2021**, *32* (3), 392−406.
(72) Burn, C. R.; Lewkowicz, A. G. Retrogressive Thaw Slumps. *Can. Geogr.* **1990**, *34* (3), 273−276.
(73) Gooseff, M. N.; Balser, A.; Bowden, W. B.; Jones, J. B. Effects of Hillslope Thermokarst in Northern Alaska. *EOS, Trans., Am. Geophys. Union* **2009**, *90* (4), 29−30.
(74) Bowden, W. B.; Gooseff, M. N.; Balser, A.; Green, A.; Peterson, B. J.; Bradford, J. Sediment and Nutrient Delivery from Thermokarst Features in the Foothills of the North Slope, Alaska: Potential Impacts on Headwater Stream Ecosystems. *J. Geophys. Res. Biogeosci.* **2008**, *113* (G2), No. 1, DOI: 10.1029/2007JG000470.
(75) Abbott, B. W.; Jones, J. B. Permafrost Collapse Alters Soil Carbon Stocks, Respiration, CH4, and N2O in Upland Tundra. *Global Change Biol.* **2015**, *21* (12), 4570−4587.
(76) McCrystall, M. R.; Stroeve, J.; Serreze, M.; Forbes, B. C.; Screen, J. A. New Climate Models Reveal Faster and Larger Increases in Arctic Precipitation than Previously Projected. *Nat. Commun.* **2021**, *12* (1), No. 6765.
(77) Chen, Y.; Lara, M. J.; Jones, B. M.; Frost, G. V.; Hu, F. S. Thermokarst Acceleration in Arctic Tundra Driven by Climate Change and Fire Disturbance. *One Earth* **2021**, *4* (12), 1718−1729.
(78) Thompson, A.; Chadwick, O. A.; Rancourt, D. G.; Chorover, J. Iron-Oxide Crystallinity Increases during Soil Redox Oscillations. *Geochim. Cosmochim. Acta* **2006**, *70* (7), 1710−1727.
(79) Aeppli, M.; Vranic, S.; Kaegi, R.; Kretzschmar, R.; Brown, A. R.; Voegelin, A.; Hofstetter, T. B.; Sander, M. Decreases in Iron Oxide Reducibility during Microbial Reductive Dissolution and Transformation of Ferrihydrite. *Environ. Sci. Technol.* **2019**, *53* (15), 8736−8746.
(80) Sobolev, D.; Roden, E. E. Evidence for Rapid Microscale Bacterial Redox Cycling of Iron in Circumneutral Environments. *Antonie Van Leeuwenhoek* **2002**, *81* (1), 587−597.
(81) Herndon, E.; Kinsman-Costello, L.; Godsey, S. Chapter 12: Biogeochemical Cycling of Redox-Sensitive Elements in Permafrost-Affected Ecosystems. In *Biogeochemical Cycles; Geophysical Monograph Series*; American Geophysical Union (AGU), 2020; pp 245−265.

https://doi.org/10.1021/acs.est.3c09072
Environ. Sci. Technol. XXXX, XXX, XXX−XXX